

Document downloaded from:

<http://hdl.handle.net/10251/63320>

This paper must be cited as:

Pulido Junquera, MA.; Concepción Heydorn, P.; Boronat Zaragoza, M.; Corma Canós, A. (2012). Aerobic epoxidation of propene over silver (111) and (100) facet catalysts. JOURNAL OF CATALYSIS. 292:138-147. doi:10.1016/j.jcat.2012.05.006.



The final publication is available at

<http://dx.doi.org/10.1016/j.jcat.2012.05.006>

Copyright Academic Press; Elsevier

Additional Information

# “Aerobic epoxidation of propene over silver (111) and (100) facet catalysts”

Angeles Pulido, Patricia Concepción, Mercedes Boronat, Avelino Corma\*

*Instituto de Tecnología Química, Universidad Politécnica de Valencia-Consejo Superior  
de Investigaciones Científicas, Av. de los Naranjos s/n, E-46022 Valencia, Spain*

acorma@itq.upv.es

Telf: 34 96 387 7824

FAX: 34 96 387 9444

## **Abstract**

Catalytic performance of single crystal Ag(100) and Ag(111) catalysts for propene oxidation has been investigated by means of Raman spectroscopy and mass spectrometry, and the energy profile has been obtained at the DFT-D level. It has been theoretically found, and confirmed by Raman spectroscopy, that Ag(100) surface is more reactive towards O<sub>2</sub> dissociation than Ag(111), and that adsorbed oxo-species are more strongly bonded to the Ag(100) facet. The higher selectivity towards propylene oxide (PO) observed for the Ag(100) catalyst can be rationalized from theoretical calculations indicating that the activation barriers for formation of the allylic intermediate -precursor of combustion products- are rather similar on both silver surfaces, whereas energy barriers on the reaction pathways for formation of PO and carbonylic products (acetone and propanal) are systematically smaller on the Ag(100) surface.

**Keywords:** Propylene epoxidation, Ag(100), Ag(111), Mass spectrometry, Raman spectroscopy, DFT calculations, Propylene oxide selectivity, Oxygen activation.

## 1. Introduction

Propylene oxide (1,2-epoxypropane) is a valuable precursor in the chemical industry of polymers,<sup>[1]</sup> and large efforts have been devoted in the last years to develop a cost-efficient and environmentally friendly synthetic route that replaces the production processes based on chlorohydrin and peroxides.<sup>[2-7]</sup>

Interesting alternative routes for the production of propylene oxide are based on direct epoxidation of propylene with molecular oxygen,<sup>[8-10]</sup> in a similar way as ethylene oxide is nowadays industrially produced,<sup>[11-15]</sup> or otherwise with hydrogen peroxide formed "in situ" on gold and palladium based catalysts.<sup>[16-19]</sup> In ethylene epoxidation, selectivities higher than 80% are obtained using Ag/ $\alpha$ -alumina catalysts, and increased attention has been paid to silver based catalyst for production of propylene oxide by direct epoxidation using molecular oxygen. However, selectivity towards propylene oxide during epoxidation with air is usually lower than 40% at 10% conversion,<sup>[6-7,20-21]</sup> which makes industrial implementation not viable.

After extensive theoretical and experimental investigations of the ethylene epoxidation process over silver-based catalysts<sup>[6,12,22-32]</sup>, a fairly good understanding of the reaction mechanism,<sup>[22-30]</sup> the role of catalyst promoters (such as chlorine and alkali metals)<sup>[6,12]</sup> and other factors such as catalyst particle size, shape and morphology<sup>[31-32]</sup> on the catalytic performance has been achieved. Direct ethylene and propylene epoxidation over silver-based catalysts using oxygen as oxidizing agent are generally assumed to follow the same reaction pathway, which is schematically shown in Scheme 1. The mechanism starts with olefin adsorption on the oxidized silver surface, atomic oxygen being the active species.<sup>[22,27,33]</sup> Activation of the allylic proton (step A) leads to formation of a radical intermediate that subsequently would generate acrolein and/or CO<sub>2</sub>, depending on the operating reaction conditions.<sup>[7,33-37]</sup> Activation of the primary

(step C) or secondary (step B) vinylic carbon atoms ends up with formation of a cyclic structure commonly referred as oxametallacycle or OMMP, where M stands for the metal atom inserted and the last letter is the initial letter for the olefin precursor, propylene (P) in this case. From the OMMP complexes, carbonyl species are formed by transferring a vinylic hydrogen (steps D and F); whereas by epoxidation (step E) propylene oxide is obtained. The low selectivity of silver-based catalysts towards propylene epoxide has been related to the limited formation of the OMMP precursors (steps B and C), while the competitive allylic hydrogen abstraction (step A) is usually kinetically and thermodynamically more favorable.<sup>[33-34,36-37]</sup> In the case of ethylene, (R = H), the absence of allylic hydrogen atoms drastically decreases the formation of the radical intermediate that would arise from vinylic hydrogen abstraction.

The influence of catalyst morphology on the selectivity towards ethylene epoxide on silver-based catalysts has been investigated, and a better performance of the (100) surface as compared to the most stable (111) surface has been reported.<sup>[31-32]</sup> Direct propylene epoxidation by molecular oxygen over silver-based catalysts has also been investigated<sup>[6,38-50]</sup> but, since conventionally synthesized catalysts are highly polycrystalline –exhibiting several crystallographic facets and showing broad particle size distribution–, a detailed understanding of the nature of the selective active sites becomes a quite challenging task. It is therefore of interest to gain an atomistic view of the catalytic centers and of the reaction mechanism by means of theoretical calculations.<sup>[28,35,51-59]</sup> The reaction mechanism for propylene oxidation on different metal (111) surfaces has been recently investigated using a periodic DFT model,<sup>[57-58]</sup> while only some steps of the reaction path have been studied on silver (100) and (110) surfaces.<sup>[59]</sup>

Thus, with the aim of getting a better understanding of the role of surface morphology on the propylene oxidation process, the direct oxidation of propylene by oxygen catalyzed by Ag(111) and Ag(100) surfaces has been investigated in the present contribution by means of a combined experimental and theoretical study. In a first step, theoretical DFT calculations on periodic slab models of the Ag(111) and Ag(100) surfaces were used to locate the intermediate and transition state structures along the reaction pathway for propylene oxidation mechanism. Then, the catalytic performance of Ag(111) and Ag(100) monocrystals was followed by Raman spectroscopy coupled to a mass spectrometer for analysis of reaction products. Low oxygen coverage has been selected in the experimental study to avoid severe catalyst reconstruction.<sup>[39,50]</sup> Based on these results, the better catalytic performance of Ag(100) facet towards propylene oxide production is discussed.

## 2. Materials and Methods

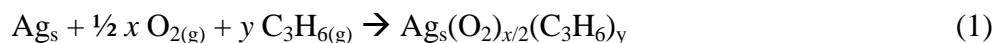
### 2.1. Computational methods and models

A five-layer periodic slab model was used to investigate silver (100) and (111) surface catalysts; referred to as Ag<sub>s</sub>(100) and Ag<sub>s</sub>(111), respectively. The unit cell (UC) volume of the silver bulk model (Fm $\bar{3}$ m space group) was obtained from a Birch-Murnaghan fit,<sup>[60-61]</sup>  $a = 2.941 \text{ \AA}$ . The fixed-volume UC of Ag<sub>s</sub>(100) model ( $a = 8.823 \text{ \AA}$  and  $V = 1943 \text{ \AA}^3$ ) and Ag<sub>s</sub>(111) model ( $a = 8.823 \text{ \AA}$  and  $V = 1685 \text{ \AA}^3$ ) were used for periodic DFT calculations. A vacuum region of about  $15 \text{ \AA}$  ( $c = 25.0 \text{ \AA}$ ) was used to avoid interaction between periodically repeated images. A UC composition of O<sub>n</sub>(C<sub>3</sub>H<sub>6</sub>)<sub>m</sub>[Ag<sub>45</sub>] ( $n = 0, 1$  and  $2$  and  $m = 0$  and  $1$ ) was used, unless stated otherwise.

The structures of all complexes were optimized at the periodic DFT level (PW91 functional)<sup>[62-63]</sup>, using a projector-augmented-wave method (PAW) by Blöchl<sup>[64]</sup> as

adopted by Kresse and Jourbert,<sup>[65]</sup> and a plane-wave basis set with a kinetic energy cut-off of 400eV. Calculations on Ag<sub>s</sub>(100) and Ag<sub>s</sub>(111) slab models were performed with a  $3 \times 3 \times 1$  **k**-mesh that corresponds to a number of 5 irreducible **k**-points. Spin polarized calculations were performed. Geometry optimizations were performed fixing the coordinates of the silver atoms in the two lowermost layers, whereas all other atoms were fully relaxed until forces were below 0.015 eV Å<sup>-1</sup>. The optimization of the transition state structures was performed with the dimer method using only first derivatives.<sup>[66]</sup> The calculations were performed using the VASP program.<sup>[67]</sup> Frequency analysis was carried out on all the intermediate and transition state structures at the equilibrium geometries identifying them as zero or first order stationary points, respectively. The vibrational frequencies were evaluated in a subspace of the Hessian matrix containing the degrees of freedom of the C, H and O atoms (6- and 30-dimensional Hessian for the O<sub>2</sub> and C<sub>3</sub>H<sub>6</sub>O complexes, respectively), with the second derivatives calculated numerically with ±0.01 displacements. Comparison of absolute experimental and DFT calculated frequencies, ω<sub>OO</sub>, should be done with caution and it is necessary to take into account that vibrational frequencies were evaluated: 1) under the harmonic approximation, 2) using a subspace of the hessian matrix and 3) numerically because the analytic second partial derivatives of the system energy are not available in the VASP code. Moreover, we are dealing with a surface with a large dipole under periodic boundary conditions and although polarization corrections have been taken into account, forces could be affected by finite size errors.

The interaction energies of the O<sub>2</sub> and C<sub>3</sub>H<sub>6</sub>O complexes with the silver surfaces were evaluated for the process described in eq. (1):



,with  $x = 0, 1$  and  $2$  and  $y = 0$  and  $1$ , where Ag<sub>s</sub> represents the silver surface model.

The periodic DFT model employed in the present study is expected to mimic the monocrystal catalysts. However, the method (PW91 functional) is expected to have a sizable error describing the metal-adsorbate interaction, and a more reliable description is expected when the hybrid B3LYP<sup>[68-69]</sup> functional is used. Small cluster calculations (AgO<sub>2</sub> and AgC<sub>2</sub>H<sub>4</sub>) show that interaction energies calculated using the hybrid B3LYP functional and including dispersion corrections are in reasonable good agreement with those obtained at the coupled-cluster level including single and double excitations and accounting for triple excitation at the perturbation theory level, CCSD(T)<sup>[70-71]</sup> method (See Supporting information for additional details). A correction scheme was then used to correct the relative energies calculated at the PW91 level,  $\Delta E_{\text{PW91}}$ . A silver cluster (Ag<sub>17</sub>) was used as silver surface model (Ag<sub>s</sub> in eq. 1) to calculate the electronic interaction energies at the PW91 ( $\Delta E_{\text{PW91}}$ ) and B3LYP ( $\Delta E_{\text{B3LYP}}$ ) levels. The single-point-energy calculations were performed at the periodic PW91 optimized geometries. Correlation-consistent valence-triple- $\xi$ -plus polarization function basis set for the C, H and O atoms and the relativistic effective-core pseudopotential (with substitution of 28 inner electrons) and valence (8s7p6d2f) basis sets on Ag<sup>[72-74]</sup> were used in cluster model calculations, performed with the Gaussian 09 program<sup>[75]</sup>. To get an estimate of the B3LYP interaction energy calculated with the periodic DFT model ( $\Delta E_{\text{B3LYP}}$ ) the B3LYP correction ( $\Delta E_{\text{B3LYP}} - \Delta E_{\text{PW91}}$ ) was added to the electronic PW91 interaction energy,  $\Delta E_{\text{PW91}}$ . Intermolecular (dispersion) interaction energies ( $\Delta E_{\text{D}}$ ) were evaluated using the DFT-D3 method<sup>[76-77]</sup> (at the periodic PW91 optimized geometries) and added to the B3LYP interaction energies,  $\Delta E_{\text{B3LYP-D}}$ .

## 2.2. Materials and experimental methods

### 2.2.1. Materials.

Disc shaped Ag(111) and Ag(100) crystals (diameter 10mm, thickness 2mm) were purchased from Goodfellow. The crystals were inserted in a Linkam cell (FTIR 600), for *in situ* Raman studies, connected through a capillary to a mass spectrometer (Balzers, QMG 220M1) for catalytic studies.

### 2.2.2. Raman spectroscopy.

Raman spectra were recorded using a 514 nm laser excitation on a Renishaw Raman Spectrometer (“*in via*”) equipped with a CCD detector. The laser power on the sample was 25 mW and a total of 20 acquisitions (200s exposure time) were taken for each spectra. In some cases analysis on different sample positions were recorded (spectral resolution  $\sim 1\mu\text{m}$ ). Previous Raman studies have shown that a minimum temperature of 200°C is necessary to remove the organic overlayer present on the catalysts surfaces, and therefore the samples were cleaned in an oxygen flow (20ml/min of 40% O<sub>2</sub>/Ar) at 200°C prior to the *in situ* Raman studies. The temperature range for the experiments (200-250°C) was chosen to limit oxygen diffusion into the bulk and the severe surface reconstruction described in the literature.<sup>[39,50]</sup>

### 2.2.3. Mass spectrometry.

First, silver (100) and (111) single crystal catalysts were activated in an O<sub>2</sub> flow at 250 °C during 2h and after this, samples were cooled down to 200 °C. Then, propylene oxidation reaction was performed in the 200-275°C temperature range, keeping 45 min at each temperature, and using a 25 ml/min total flow of C<sub>3</sub>H<sub>6</sub>:O<sub>2</sub>:Ar with molar ratio: 2:1:7.6. The reaction products were followed by mass spectrometry in the multi-ion mode (MID) using a Balzer (QMG 220M1) spectrometer. All catalytic tests were performed in absence of visible light. The selection of m/z values was based on the analog scan performed for the main reaction products expected (acrolein, acetone, propylene oxide, propanal, CO and CO<sub>2</sub>) summarized in Table S1 in the Supporting



Information. For quantitative data analysis, calibration of each product conversion was done by measuring the increment in the  $m/z$  value characterizing each product and normalizing versus the propene signal at 0% conversion. In the calibration measurements, the reaction feed was used as reference flow, passing the Ar flow through a saturator working at specified temperatures in order to achieve yields to each product in the 0-5% range.

### **3. Results and discussion**

The first step in the global epoxidation mechanism, activation and dissociation of molecular  $O_2$  into adsorbed atomic O, was investigated on Ag(111) and Ag(100) facets by means of periodic DFT calculations and Raman spectroscopy. The differences in the ability to dissociate  $O_2$  and in the stability of atomic O adsorbed on the two crystallographic facets were analyzed in depth and are presented first. Then, the reaction mechanism for propene epoxidation over partially oxidized Ag(100) and Ag(111) surface models was obtained from DFT calculations and is described in detail. Finally, the catalytic performance of Ag(111) and Ag(100) monocrystals was followed by Raman spectroscopy and mass spectrometry, and the results obtained are shown and discussed together with the DFT findings.

#### **3.1. Oxygen activation on Ag(100) and Ag(111) catalysts**

The mechanism of  $O_2$  dissociation on Ag(100) and Ag(111) surfaces was theoretically investigated using a periodic DFT model. The intermediate and transition state structures along the reaction pathway on both surfaces were identified and characterized by means of frequency calculations at the PW91 level, and relative energies with respect to gas phase  $O_2$  ground state and the silver surface were calculated at the PW91 ( $\Delta E_{PW91}$ ), B3LYP ( $\Delta E_{B3LYP}$ ) and B3LYP with dispersion correction

( $\Delta E_{\text{B3LYP-D}}$ ) levels, as described in Section 2. Equilibrium geometries at the periodic PW91 level are depicted in Figure 1,  $\Delta E_{\text{B3LYP-D}}$  relative energies are shown in Figure 2 and are discussed in the text unless otherwise stated and  $\Delta E_{\text{PW91}}$  and  $\Delta E_{\text{B3LYP}}$  relative energies can be found as Supplementary Information.

Among the several  $\text{O}_2$  adsorption complexes investigated on the Ag(100) surface with oxygen coverage 0.222, the most stable one (species **1** in Figure 2) has each of the two oxygen atoms bridged between two silver atoms (Figure 1b). The O—O bond has been activated, as reflected in the lengthening of the O—O distance by 0.235 Å with respect to that of gas phase  $\text{O}_2$  molecule, and 65  $\text{kJ mol}^{-1}$  are released in the adsorption process.  $\text{O}_2$  dissociation occurs via transition state structure **2**, in which the optimized O...O distance of 2.206 Å indicates that the O—O bond is already broken (Figure 1c). After dissociation the two oxygen atoms are located at hollow sites, (species **3** in Figure 2) and exhibit a four-fold coordination to silver atoms with average Ag—O distances of 2.26 Å (Figure 1d).  $\text{O}_2$  dissociation (**1**→**3**) is exothermic by -119  $\text{kJ mol}^{-1}$  and requires an activation energy of about 90  $\text{kJ mol}^{-1}$ .

The relative energy of the most stable  $\text{O}_2$  adsorption complex on the Ag(111) surface (species **1'** in Figure 2) with respect to gas phase  $\text{O}_2$  and the silver surface is only -21  $\text{kJ mol}^{-1}$ , and the activation of the O—O bond is not as large as on the Ag(100) surface, as indicated by an increase in the O—O distance of only 0.082 Å with respect to gas phase  $\text{O}_2$  (Figure 1f). Oxygen dissociation on the Ag(111) surface (**1'** → **3'**) occurs through transition state structure **2'**, in which the O—O distance is 1.847 Å (Figure 1g). After dissociation, the two oxygen atoms occupy *fcc* and *hcp* sites, and are three-fold coordinated to Ag atoms with average O—Ag distances of 2.12 and 2.11 Å, respectively (Figure 1h). The activation energy required to dissociate  $\text{O}_2$  on the Ag(111)

surface is about  $20 \text{ kJ mol}^{-1}$  larger than on the Ag(100) surface, and the reaction is exothermic by  $-101 \text{ kJ mol}^{-1}$ .

Then, the oxygen dissociation ability of silver (100) and (111) crystallographic facets was investigated using Raman spectroscopy. Oxygen activation on Ag(100) and Ag(111) monocrystals was performed at increasing temperature in the range  $200 - 250 \text{ }^\circ\text{C}$ , and the recorded Raman spectra are shown in Figure 3. On Ag(111) monocrystal, oxygen activation starts at  $225^\circ\text{C}$ , and bands at  $475, 875, 957$  and  $990 \text{ cm}^{-1}$  are observed (black line in Figure 3a). When temperature is raised to  $250 \text{ }^\circ\text{C}$  (red line in Figure 3a), two new weak bands at  $603$  and  $790 \text{ cm}^{-1}$  appear. Oxygen activation on the Ag(100) facet starts at a lower temperature,  $200 \text{ }^\circ\text{C}$  (green line in Figure 3b), and not only the bands at  $470, 870$  and  $957 \text{ cm}^{-1}$  also present on Ag(111) monocrystal at  $225^\circ\text{C}$ , but also the bands at  $604$  and  $802 \text{ cm}^{-1}$  (that on Ag(111) appear at  $250^\circ\text{C}$ ) and a new band at  $338 \text{ cm}^{-1}$ , are already observed on Ag(100) facet at  $200 \text{ }^\circ\text{C}$ . This is in agreement with DFT data that predict a lower energy barrier ( $\sim 20 \text{ kJ mol}^{-1}$ ) for oxygen activation on the Ag(100) than on the Ag(111) surface model. When temperature is raised, the intensity of all Raman bands on Ag(100) monocrystal increase (black and red lines in Figure 3b), and at  $250 \text{ }^\circ\text{C}$  the Raman spectra on both Ag(100) and Ag(111) surfaces show quite similar oxygen species.

The bands at higher frequencies,  $957$  and  $990 \text{ cm}^{-1}$ , are assigned to the  $\nu(\text{O}=\text{O})$  stretching mode of adsorbed molecular oxygen, on the basis of previously reported values ranging between  $983$  and  $960 \text{ cm}^{-1}$ .<sup>[46,49]</sup> It is known that the activation of molecular  $\text{O}_2$  is due to charge transfer from the metal surface to the  $\pi^*$  molecular orbital of adsorbed  $\text{O}_2$ , that leads to a weakening of the  $\text{O}-\text{O}$  bond and consequently to an increase in the  $\text{O}-\text{O}$  bond length. A series of  $\text{O}_2$  adsorption complexes at oxygen coverage between  $0.222$  and  $0.444$  were obtained over Ag(100) and Ag(111) surfaces at

the periodic PW91 level, and the optimized O—O bond lengths, the calculated  $\omega_{OO}$  stretching frequencies, and the net atomic charges are given in Figure S4 and Table S4 in the Supporting Information. As mentioned before, the calculated harmonic  $\omega_{OO}$  vibrational frequencies suffer a certain deviation from the experimental values due in part to the neglect of anharmonicity effects, and the use of a subspace of the hessian matrix and a polarized surface model. While these approximations do not allow for a direct comparison of the absolute values of the calculated  $\omega_{OO}$  vibrational frequencies with experimental values, they do not prevent a further analysis of the trends observed. Thus, a strong correlation was found between the calculated  $\omega_{OO}$  stretching frequencies and the net atomic charge on adsorbed O<sub>2</sub>: as O—O bond activation increases due to charge transfer to O<sub>2</sub>, the calculated  $\omega_{OO}$  stretching frequencies decrease (see Figure S5). This is caused either by higher oxygen loading, resulting in less charge donation from silver to  $\pi^*$  molecular orbital of adsorbed O<sub>2</sub>, or by surface topology, with Ag(111) surface leading to a lower degree of O<sub>2</sub> activation. Thus, the presence of several bands in the region of the  $\nu(\text{O}=\text{O})$  stretching mode in the Raman spectra obtained for Ag(111) monocrystal, centered at 957 and 990 cm<sup>-1</sup>, is associated to adsorbed O<sub>2</sub> species with different degree of activation. On Ag(100) monocrystal, only the lower frequency band at 957 cm<sup>-1</sup> is observed, indicating a higher degree of O<sub>2</sub> activation on this surface.

The bands at 870-875 cm<sup>-1</sup> could be associated to the bending vibration of Ag-OH hydroxyl groups<sup>[42,78]</sup> generated in the presence of ppm amounts of H<sub>2</sub>O in the gas flow, while the low frequency bands at 470-475 cm<sup>-1</sup> fall in the region of the Ag-O stretching vibration that can be attributed to atomic oxygen species.<sup>[39,46]</sup> On the other hand, the bands at 338, 603-604 and 790-802 cm<sup>-1</sup> observed on Ag(100) at 200°C and on Ag(111) at 250°C are associated to subsurface oxo-species and to surface oxygen species (labeled O<sub>γ</sub>) stabilized by the presence of subsurface oxygen,<sup>[39,45-46,48]</sup> and

indicate that oxygen diffusion into the bulk takes place on Ag(100) at a much lower temperature than on Ag(111) facet.

To investigate the stability of the adsorbed oxygen species, an inert gas was flown over the oxidized silver surfaces. After doing that, the intensity of all Raman bands strongly decrease on Ag(111) surface (blue line in Figure 3a) while they are still present on Ag(100) surface (blue line in Figure 3b). This indicates a higher stability of all adsorbed oxygen species on the Ag(100) as compared to the Ag(111) surface, in agreement with the DFT results that predicted a larger stability stability (by more than  $40 \text{ kJ mol}^{-1}$ ) of the adsorbed oxo-species on the Ag(100) surface.

Finally, it should be mentioned that the structure and stability of oxygen adatoms obtained in this work are within the range of previously reported data and show a similar trend with oxygen coverage. Most theoretical studies dealing with oxygen adsorption on silver surfaces focus on the structure and stability of oxygen adatoms at varying oxygen coverage. Thus, the most stable location of oxygen atoms on a clean Ag(100) surface is at hollow sites coordinated to four silver atoms, with the GGA calculated interaction energies decreasing from  $-95$  to  $-24 \text{ kJ mol}^{-1}$  as oxygen coverage increases from 0.111 to 1.0.<sup>[51,55-56,79]</sup> The O...Ag(100) interaction energies per oxygen atom obtained in this work at the PW91 level are  $-84$  and  $-91 \text{ kJ mol}^{-1}$  for oxygen coverage of 0.222 and 0.111, respectively, in agreement with previous work. The most stable location for oxygen atoms on Ag(111) surface is on three-fold coordinated *fcc* hollow sites, with interaction energies smaller than on Ag(100) surface<sup>[59]</sup>. Dissociation of molecular  $\text{O}_2$  on Ag(111) has been previously investigated at the PW91 level,<sup>[28]</sup> and the activation barrier reported for a oxygen coverage of 0.125,  $62 \text{ kJ mol}^{-1}$ , is in good agreement with our calculated activation energy ( $55 \text{ kJ mol}^{-1}$ ) at the same PW91 level and at an oxygen coverage of 0.222. A much higher activation barrier ( $171 \text{ kJ mol}^{-1}$ ) has

been reported for O<sub>2</sub> dissociation over a Ag(111) surface with a oxygen coverage of 0.222,<sup>[56]</sup> obtained at the periodic PBE level, using PAW-projected wave functions and non-spin-polarized calculations. The large difference between this activation barrier and those reported by Bocquet *et al.*<sup>[28]</sup> and found in this work has been discarded to be due to methodology selection (PBE vs. PW91 functional or inclusion of spin polarization), but can probably attributed to a different transition state structure in ref. [56].

### 3.2. Propylene oxidation on Ag(100) and Ag(111) catalysts.

#### 3.2.1. Theoretical study of reaction mechanism on Ag(100)

The equilibrium geometries of the intermediate and transition state structures along the reaction pathways for propylene oxidation on the Ag(100) surface obtained at the PW91 level are depicted in Figure 4, and relative energies (with respect to gas phase C<sub>3</sub>H<sub>8</sub> and O<sub>2</sub> molecules and the silver surface) calculated at the B3LYP-D level, ( $\Delta E_{\text{B3LYP-D}}$ ) are shown in Figure 5. For oxygen coverage of 0.111, the most stable location of the oxygen atom is at the hollow site, coordinated to four silver atoms (see Figure 1) and the calculated relative energy  $\Delta E_{\text{B3LYP-D}}$  is -99 kJ mol<sup>-1</sup>.

All pathways start with propylene adsorption close to an oxygen atom adsorbed on the silver surface and, as mentioned in the introduction and shown in Scheme 1, propylene can interact with the adsorbed oxygen atoms in three different ways: 1) via one of the hydrogen atoms of the methyl group (R = CH<sub>3</sub>), starting the *allyl* route (step A in Scheme 1), 2) via the secondary vinylic carbon (C<sub>b</sub>), starting the *branched* route where branched intermediates and products (acetone) are formed (step B in Scheme 1), and 3) via the primary vinylic carbon (C<sub>a</sub>), starting the *linear* route that leads to formation of linear intermediates and products (propanal) (step C in Scheme 1). Propylene adsorption on the oxidized silver surface is exothermic by 33 kJ mol<sup>-1</sup> in all cases, regardless the adsorbed propylene complex formed.

The *allyl* route starts with propylene adsorption via CH...O interaction, forming the intermediate species **5** in which the optimized H—O distance is 2.353 Å (see Figure 4a). Hydrogen transfer to the surface oxygen atom occurs through transition state **6**, where the C—H and O—H distances are 1.338 Å and 1.266 Å, respectively, and leads to formation of the allylic radical species **7**. The process (**7** → **9**) is endothermic by 2 kJ mol<sup>-1</sup> and involves an activation barrier of only 29 kJ mol<sup>-1</sup>.

Propylene adsorption via C<sub>b</sub>...O interaction is the first step in the *branched* route, and results in formation of species **8** (Figure 4b). Two different five-member oxametallacycle intermediates can be formed from structure **8** by bonding the primary C<sub>a</sub> atom to a surface silver atom and the secondary C<sub>b</sub> atom to the adsorbed oxygen atom. The two structures mainly differ in the location of the oxygen atom: at the hollow site in structure **10** and bridged between two silver atoms in species **14**. These oxametallacycle intermediates are formed through transition states **9** and **13**, respectively, in which the O—C<sub>b</sub> interaction is already quite strong and the Ag—C<sub>a</sub> bonds are almost formed (Figure 4b). Formation of the two branched oxametallacycle intermediates is endothermic, with reaction energies within 3-8 kJ mol<sup>-1</sup>, and involves activation barriers of 48 (**8** → **10**) and 57 (**8** → **14**) kJ mol<sup>-1</sup>. The optimized geometries of transition states **9** and **13** are quite similar, but the calculated energies and the frequency analysis show that they are different structures.

Acetone adsorbed on the silver surface (species **12**) is formed from the oxametallacyclic intermediate **10** by a H shift from C<sub>b</sub> to C<sub>a</sub> via transition state **11**, in which the C<sub>b</sub>—H and O—C<sub>b</sub> bond distances are 1.264 and 1.306 Å, respectively. The calculated activation barrier for this step (**10** → **12**) is 70 kJ mol<sup>-1</sup>, and more than 140 kJ mol<sup>-1</sup> are released in the process. In the same *branched* route, the oxametallacycle intermediate **14** is oxidized to the epoxide **16** through transition state **15**, in a process

involving the breaking of the Ag—C<sub>a</sub> bond and the formation of a (-C<sub>b</sub>OC<sub>a</sub>-) cycle. The calculated activation barrier for epoxidation (62 kJ mol<sup>-1</sup>) is slightly lower than that for acetone formation, and the process is exothermic by -25 kJ mol<sup>-1</sup>.

The *linear* route for propylene oxidation on silver (100) surface starts with propylene adsorption via C<sub>a</sub>...O interaction, yielding structure **17** (see Figure 4c). Reaction pathways on the *linear* and *branched* routes are very much alike, and involve in both cases two different five-member oxametallacycle intermediates that finally lead to either the epoxide or a molecule having a carbonyl group (propanal or acetone). The two oxametallacycle intermediates formed in the *linear* route by bonding of the primary C<sub>a</sub> atom to adsorbed O and the secondary C<sub>b</sub> atom to a surface silver atom are structure **19**, with the O atom placed at a hollow site, and species **23** with the O atom bridged between two silver atoms. These two intermediates are ~ 25 kJ mol<sup>-1</sup> less stable than adsorbed propylene **17**, and they are formed through transition states **18** and **22** with activation barriers of 59 and 64 kJ mol<sup>-1</sup>, respectively. The oxametallacycle intermediate **19** leads to formation of the carbonylic product propanal (**21**) by hydrogen shift from C<sub>a</sub> to C<sub>b</sub> via transition state **20** (Figure 4c). The process (**19** → **21**) is highly exothermic, with calculated reaction energy of -137 kJ mol<sup>-1</sup>, and requires activation energy of 64 kJ mol<sup>-1</sup>. Finally, the desired epoxide (species **25**) is also formed in the *linear* route from structure **23** via transition state **24**, in which the Ag—C<sub>b</sub> bond is already broken and the O atom is directly bonded to C<sub>a</sub> and already interacting with C<sub>b</sub>. The barrier for epoxide formation is 48 kJ mol<sup>-1</sup> which is noticeably lower than that for propanal formation, and 48 kJ mol<sup>-1</sup> are released in this step.

It can be concluded from this part of the study that the rate determining step in the propylene oxidation mechanism is the dissociation of molecular O<sub>2</sub> into two adsorbed oxygen atoms. After propylene adsorption on the oxygen-covered surface, the



hydrogen step transfer starting the *allyl* route involves the lowest activation barrier (29 kJ mol<sup>-1</sup>), and the reaction is thermoneutral. Formation of the oxametallacycle intermediates is slightly endothermic and involves activation barriers between 48 and 64 kJ mol<sup>-1</sup>. Once the oxametallacycles are formed, the activation energies necessary to produce propylene oxide, acetone and propanal (within 48 to 70 kJ mol<sup>-1</sup>) are comparable to the energy required to form the oxametallacyclic structures.

### 3.2.2. Theoretical study of reaction mechanism on Ag(111)

The mechanism of propylene epoxidation over Ag(111) has been previously investigated using periodic DFT. A really high activation barrier (120 kJ mol<sup>-1</sup>) was reported by López *et al.*<sup>[57]</sup> for formation of a branched oxametallacycle intermediate, and therefore only the *allyl* and the *linear* routes were investigated in that work.<sup>[57]</sup> However, taking into account the similarities between the reaction pathways for: i) the *linear* and *branched* routes on the Ag(100) surface, and ii) the *linear* route on the Ag(111)<sup>[57]</sup> and Ag(100) surfaces, we have considered pertinent to re-investigate the *branched* route on the Ag(111) surface. For comparison, the *allyl* route on the Ag(111) surface has also been calculated in this work.

For an oxygen coverage of 0.111, the most stable location of the oxygen atom is at a hollow *fcc* site directly coordinated to three silver atoms (Figure 1) and the calculated relative energy  $\Delta E_{\text{B3LYP-D}}$  is -77 kJ mol<sup>-1</sup> (Table S3 in the Supporting Information). The equilibrium geometries of the intermediate and transition state structures along the *allyl* and *branched* pathways for propylene oxidation on Ag(111) surface obtained at the PW91 level are depicted in Figure 6, and Figure 5b shows the  $\Delta E_{\text{B3LYP-D}}$  calculated relative energies.

The *allyl* route starts with propylene adsorption on the oxidized silver (111) surface leading to formation of complex **5'** (Figure 6a). The optimized O--H distance in

species **5'** is 2.092 Å, that is 0.261 Å shorter than on the equivalent complex **5**, and the adsorption process on the Ag(111) surface is 10 kJ mol<sup>-1</sup> more exothermic than on the Ag(100) surface (Figure 5). The allylic radical species **7'** is formed on the Ag(111) surface via transition state **6'**, with an activation energy of 33 kJ mol<sup>-1</sup> and releasing 27 kJ mol<sup>-1</sup> at the B3LYP-D level. The PW91 calculated activation barrier is 24 kJ mol<sup>-1</sup>, in very good agreement with that previously reported by López *et al.*, 29 kJ mol<sup>-1</sup><sup>[57]</sup>.

The first step in the *branched* route is formation of species **8'** by propylene adsorption on the oxidized Ag(111) surface via C<sub>b</sub>...O interaction (Figure 6b), this step being exothermic by 43 kJ mol<sup>-1</sup>. A five-member oxametallacycle species **10'**, that is 21 kJ mol<sup>-1</sup> more stable than adsorbed propylene, is formed via transition state TS **9'** with an activation barrier of 56 kJ mol<sup>-1</sup>. The activation energy calculated at the PW91 level is only 52 kJ mol<sup>-1</sup>, which is considerably lower than that previously reported of 117 kJ mol<sup>-1</sup><sup>[57]</sup>. Following the reaction scheme obtained on the Ag(100) surface, a second five-member oxametallacycle intermediate **14'** was searched and located on the potential energy surface, as well as the corresponding transition state **13'** involved in the process (**8'** → **14'**). However, the optimized structures and the calculated energies of species **10'** and **14'** (and of **9'** and **13'**) are almost equivalent, suggesting the possibility that only one *branched* oxametallacycle intermediate is formed on Ag(111) surface, and further frequency analysis shows that this is indeed the case. From this *branched* oxametallacycle intermediate, acetone is formed via transition state **11'** with an activation barrier of 95 kJ mol<sup>-1</sup>, and the desired epoxide is formed via transition state **15'** in a process involving a lower activation energy, 76 kJ mol<sup>-1</sup>.

These results indicate that on Ag(111) surface, like on Ag(100), the rate determining step in the mechanism is the dissociation of molecular O<sub>2</sub>. The *allyl* route, leading to combustion products, involves the lowest activation barrier, 33 kJ mol<sup>-1</sup> and it

is kinetically favored over the OMMPs. The main difference between the two surfaces is that formation of allylic and oxametallacycle intermediates on Ag(111) are exothermic processes by 20 – 30 kJ mol<sup>-1</sup>; whereas they are thermoneutral or slightly endothermic on Ag(100). Moreover, on Ag(111) surface, formation of propylene oxide (kinetically favored) or carbonyl products require activation energies between 75 – 95 kJ mol<sup>-1</sup>; which are up to 20 kJ mol<sup>-1</sup> higher than on Ag(100) surface.

Finally, the role of the functional employed (PW91 vs. B3LYP) and dispersion energy on the calculated energy profiles for propylene oxidation on Ag(100) and Ag(111) surfaces is analyzed. Data summarized in Tables S2-S3 in the Supporting Information indicate that, in all cases, PW91 activation barriers are lower (up to 38 kJ mol<sup>-1</sup>) than those calculated at the B3LYP level. On the other hand, the influence of dispersion energies varies with the elementary step and the silver surface considered. On Ag(100), the interaction dispersion energies ( $\Delta E_D$ ) are larger for transition states, allyl and oxametallacycle intermediates than for the propylene, acetone, propanal and epoxide adsorption complexes. These differences lead to a decrease of the activation barriers in the first step of the oxidation process of about 10 kJ mol<sup>-1</sup> compared with the B3LYP values, while the activation barriers in the second step of the mechanism are up to 18 kJ mol<sup>-1</sup> larger at the B3LYP-D level than at the B3LYP level. On Ag(111) surface, the interaction dispersion energies ( $\Delta E_D$ ) for transition states, propylene adsorption complexes, allyl and oxametallacycle intermediates are similar (between -50 and -58 kJ mol<sup>-1</sup>) and, as a consequence, activation barriers only vary up to 5 kJ mol<sup>-1</sup> with respect to the B3LYP values.

From the theoretical results it would be possible to conclude that non selective oxidation will be favourable over epoxidation on Ag catalysts, regardless the crystal

orientation. However, epoxide selectivity should be larger with Ag(100) than with Ag(111) catalysts.

### 3.2.3. Raman spectroscopy and mass spectrometry

The reactivity of the oxygen species adsorbed on Ag(100) and Ag(111) monocrystals towards propylene was investigated using “*in situ*” Raman spectroscopy coupled to a mass spectrometer for analysis of the reaction products. The samples were first pre-activated in an O<sub>2</sub> flow at 250°C (see Section 2 for details) and their Raman spectra, recorded at 200°C, are shown in Figure 7 (green line). In the presence of the reactant feed, C<sub>3</sub>H<sub>6</sub>/O<sub>2</sub>/Ar flow, the intensity of the Raman bands decrease sharply on both catalysts (Figure 7, red line), indicating that reactivity of propene towards adsorbed oxygen species is high and rather similar on the two facets studied. Regeneration of the oxygen species under reaction conditions at 200°C is low on the Ag(100) facet (see the low intensity of the Raman bands in Figure 7b, red line) and does not occur on the Ag(111) facet. At 250°C oxygen species are observed on both faces (Figure 7, black line). These results agree with the DFT findings where oxygen activation is found to be the rate limiting step on both silver surfaces, with a lower energy barrier on the Ag(100) surface.

Simultaneously to the acquisition of the Raman spectra, reaction products were analyzed “on line” by mass spectrometry (Table 1). The selection of *m/z* values was based on the analog scan performed for the main reaction products expected (acrolein, acetone, propylene oxide, propanal, CO and CO<sub>2</sub>) summarized in Table S1 in the Supporting Information. Acrolein, CO<sub>2</sub> and acetone are identified by peaks at *m/z* values of 56, 44 and 43, respectively. Ionic fragmentation of propanal and propylene oxide show a very similar pattern and therefore, although the peak at *m/z* = 31 was chosen to identify propylene oxide, the formation of propanal cannot be ruled out. The

$m/z = 58$  value, used by other groups to follow the PO formation<sup>[7,35,80-81]</sup>, was discarded based on our analog scan, because this peak could also indicate formation of acetone or propanal. CO formation ( $m/z = 28$ ) cannot be excluded either. The main products identified by simultaneous monitoring of the ion current in the mass spectrometer (MID mode) during propene oxidation on single crystal silver (100) and (111) catalysts are given in Table 1.

According to our mass spectrometer analysis, on Ag(100) catalyst all products: acrolein, CO<sub>2</sub>, acetone, and propylene oxide (and/or propanal) were observed in the whole reaction temperature range investigated (200 – 275 °C). However, with Ag(111) catalyst the dominant product is CO<sub>2</sub> in the whole range of temperatures studied, indicating that only the allylic route seems to be accessible. Formation of acetone, propanal or propene oxide was ruled out because no variation in the relative intensity of the corresponding  $m/z$  peaks was detected. In our set of experiments, no increment in the intensity of the ion current in the mass spectra was observed after switching on the laser, so the contribution of photochemical paths in our measurements can be excluded.

The different selectivity observed for the single crystal (100) and (111) facet catalysts towards non-combustion products can be better understood looking at the energy profiles obtained by the DFT investigation. Activation barriers for formation of the allylic intermediate on the silver (100) and (111) surfaces are rather similar within 4 kJ mol<sup>-1</sup>. On the Ag (100) surface, reaction pathways for OMMPs formation and subsequent production of epoxide and carbonylic products (acetone and propanal) involve activation energies up to 30 kJ mol<sup>-1</sup> larger than that required to follow the allylic route, but still accessible. However, on the Ag(111) surface, the energy barriers are systematically higher (up to 25 kJ mol<sup>-1</sup>) than on the Ag(100) surface, and the larger

difference with the activation barrier on the allylic route makes the epoxidation route non accessible on Ag(111).

Moreover, the ratio between epoxide/propanal ( $m/z = 31$ ) and acetone ( $m/z = 43$ ) yields is 1:1 on the Ag(100) catalysts (see Table 1), regardless the temperature investigated. According to the energy profiles shown in Figure 5, a ratio of  $\sim 3:1$  should be expected if all the reaction pathways were accessible, because epoxide can be formed from the *lineal* and the *branched* routes and propanal and epoxide are identified by the same  $m/z$  signal. The fact of detecting acetone production in a 1:1 ratio to epoxide/propanal seems to indicate that only the *branched* route can compete with the allylic route. This is in agreement with the DFT calculations indicating that lineal OMMPs are less stable and require higher activation energies than branched OMMPs.

#### 4. Conclusions

The complete reaction pathway for propylene oxidation on Ag(100) and Ag(111) catalyst models has been investigated by means of periodic DFT calculations. The  $O_2$  dissociation ability and reactivity towards propylene of (100) and (111) silver monocrystals has been studied with Raman spectroscopy, and the product distribution at different  $O_2$  coverage and temperature has been analyzed by mass spectrometry.

It has been theoretically found, and confirmed by Raman spectroscopy, that Ag(100) surface is more reactive towards  $O_2$  dissociation and binds adsorbed oxygen atoms stronger than Ag(111) surface.  $O_2$  dissociation is the rate determining step of the whole process, and the hydrogen abstraction step starting the *allyl* route leading to formation of acrolein and finally  $CO_2$  is kinetically favored on both catalysts. However, while formation of propylene epoxide or carbonylic compounds from oxametallacycle intermediates on Ag(111) surface involves activation barriers larger than  $75 \text{ kJ mol}^{-1}$ , on

Ag(100) the activation energies involved in these processes are comparable to that required to regenerate adsorbed propylene. This means that, while on Ag(111) the only reaction pathway energetically accessible is the *allyl* route leading to combustion products, on Ag(100) surface formation of propylene oxide and carbonylic compounds can compete with this pathway. This is indeed what it is suggested by the mass spectrometry analysis, i.e., while the dominant product on Ag(111) is that formed in the *allyl* route ( $\text{CO}_2$ ), in the case of Ag(100) acetone and propylene oxide ( $m/z = 31$ ) are also observed.

## **5. Acknowledgement**

The authors thank the Spanish Science and Innovation Ministry (MAT2011-28009 and Consolider Ingenio 2010-MULTICAT, CSD2009-00050) and the Generalitat Valenciana (PROMETEO/2008/130) for financial support, and Red Española de Supercomputación (RES) and Centre de Càlcul de la Universitat de València for computational facilities and technical assistance. A. P. thanks the Spanish Science and Innovation Ministry (Juan de la Cierva program) for her fellowship.

## References

- [1] D. Kalich, U. Wiechern, J. Linder, in: 5th ed., Ullman's Encyclopeda of Industrial Chemistry: Propylene oxide, Verlag Chemie: Weinheim, Germany, 1993; Vol. A22 p. 239.
- [2] H. Mimoun, M. Mignard, P. Brechot, L. Saussine, *J. Am. Chem. Soc.* 108 (1986) 3711.
- [3] D. L. Trent, in, *Kirk-Othmer Encyclopedia of Chemical Technology: Propylene oxide*, John Wiley and Sons, 1996; Vol. 20 p.
- [4] T. Seo, J. Tsuji, U. S. Patent No. 6,646,139 (2003), to Corporation, S.
- [5] A. Tullo, *Chem. Eng. News* 82 (2004) 15.
- [6] R. M. Lambert, F. J. Williams, R. L. Cropley, A. Palermo, *J. Mol. Catal. A: Chem.* 228 (2005) 27.
- [7] T. A. Nijhuis, M. Makkee, J. A. Moulijn, B. M. Weckhuysen, *Industrial & Engineering Chemistry Research* 45 (2006) 3447.
- [8] M. Stoukides, C. Vayenas, *J. Catal.* 74 (1982) 266.
- [9] M. Akimoto, K. Ichikawa, E. Echigoya, *J. Catal.* 76 (1982) 333.
- [10] P. Geenen, *J. Catal.* 77 (1982) 499.
- [11] H. H. Voge, C. R. Adams, in, *Catalytic Oxidation of Olefins*, Elsevier, 1967; Vol. 17 p. 151-221.
- [12] J. G. Serafin, A. C. Liu, S. R. Seyedmonir, *J. Mol. Catal. A: Chem.* 131 (1998) 157.
- [13] P. A. Kilty, W. M. H. Sachtler, *Catalysis Reviews: Science and Engineering* 10 (1974) 1.
- [14] P. Hayden, R. Clayton, J. Bamforth, A. Cope, International Patent 3642 (1979), to PLC, I.
- [15] L. A. Kapicak, A. W. Naumann, T. M. Notermann, E.M. Thorsteinson, US Patent 4 994 588 (1991), to Plastics., U. C. C. a.
- [16] B. Chowdhury, J. J. Bravo-Suarez, N. Mimura, J. Q. Lu, K. K. Bando, S. Tsubota, M. Haruta, *J. Phys. Chem. B* 110 (2006) 22995.
- [17] B. Chowdhury, J. J. Bravo-Suarez, M. Date, S. Tsubota, M. Haruta, *Angew. Chem.-Int. Edit.* 45 (2006) 412.
- [18] A. M. Joshi, W. N. Delgass, K. T. Thomson, *J. Phys. Chem. C* 111 (2007) 7841.
- [19] W.-S. Lee, R. Zhang, C. Akatay, C. Baertsch, E. Stach, F. Ribeiro, N. Delgass, *ACS Catal.* 1 (2011) 1327.
- [20] F. Zemichael, A. Palermo, M. Tikhov, R. Lambert, *Catal. Lett.* 80 (2002) 93.
- [21] A. Takahashi, N. Hamakawa, I. Nakamura, T. Fujitani, *Applied Catalysis A: General* 294 (2005) 34.
- [22] R. Grant, R. Lambert, *J. Catal.* 92 (1985) 364.
- [23] G. S. Jones, M. Mavrikakis, M. A. Barteau, J. M. Vohs, *J. Am. Chem. Soc.* 120 (1998) 3196.
- [24] J. W. Medlin, M. A. Barteau, *J. Phys. Chem. B* 105 (2001) 10054.
- [25] S. Linic, M. A. Barteau, *J. Am. Chem. Soc.* 124 (2002) 310.
- [26] S. Linic, M. A. Barteau, *J. Am. Chem. Soc.* 125 (2003) 4034.
- [27] S. Linic, M. A. Barteau, *J. Catal.* 214 (2003) 200.
- [28] M.-L. Bocquet, A. Michaelides, D. Loffreda, P. Sautet, A. Alavi, D. King, *J. Am. Chem. Soc.* 125 (2003) 5620.
- [29] S. Linic, H. Piao, K. Adib, M. A. Barteau, *Angew. Chem. Int. Ed.* 43 (2004) 2918.
- [30] M.-L. Bocquet, D. Loffreda, *J. Am. Chem. Soc.* 127 (2005) 17207.



- [31] P. Christopher, S. Linic, *J. Am. Chem. Soc.* 130 (2008) 11264.
- [32] P. Christopher, S. Linic, *ChemCatChem* 2 (2010) 78.
- [33] E. A. Carter, W. A. Goddard III, *J. Catal.* 112 (1988) 80.
- [34] F. J. Williams, R. L. Cropley, O. P. H. Vaughan, A. J. Urquhart, M. S. Tikhov, C. Kolczewski, K. Hermann, R. M. Lambert, *J. Am. Chem. Soc.* 127 (2005) 17007.
- [35] Y. Lei, F. Mehmood, S. Lee, J. Greeley, B. Lee, S. Seifert, R. E. Winans, J. W. Elam, R. J. Meyer, P. C. Redfern, D. Teschner, R. Schlogl, M. J. Pellin, L. A. Curtiss, S. Vajda, *Science* 328 (2010) 224.
- [36] M. A. Barteau, R. J. Madix, *J. Am. Chem. Soc.* 105 (1983) 344.
- [37] J. T. Roberts, R. J. Madix, W. W. Crew, *J. Catal.* 141 (1993) 300.
- [38] W. X. Huang, Z. Q. Jiang, J. M. White, *Catal. Today* 131 (2008) 360.
- [39] G. I. N. Waterhouse, G. A. Bowmaker, J. B. Metson, *Appl. Surf. Sci.* 214 (2003) 36.
- [40] V. I. Bukhtiyarov, A. I. Nizovskii, H. Bluhm, M. Havecker, E. Kleimenov, A. Knop-Gericke, R. Schlogl, *J. Catal.* 238 (2006) 260.
- [41] C. Stegelmann, N. C. Schiodt, C. T. Campbell, P. Stoltze, *J. Catal.* 221 (2004) 630.
- [42] X. Bao, M. Muhler, B. Pettinger, Y. Uchida, G. Lehmppfuhl, R. Schlogl, G. Ertl, *Catal. Lett.* 32 (1995) 171.
- [43] J. Q. Lu, J. J. Bravo-Suarez, A. Takahashi, M. Haruta, S. T. Oyama, *J. Catal.* 232 (2005) 85.
- [44] P. H. McBreen, M. Moskovits, *J. Catal.* 103 (1987) 188.
- [45] X. Bao, M. Muhler, B. Pettinger, R. Schlogl, G. Ertl, *Catal. Lett.* 22 (1993) 215.
- [46] G. J. Millar, J. B. Metson, G. A. Bowmaker, R. P. Cooney, *J. Chem. Soc.-Faraday Trans.* 91 (1995) 4149.
- [47] G. J. Millar, M. L. Nelson, P. J. R. Uwins, *Catal. Lett.* 43 (1997) 97.
- [48] E. Cao, S. Firth, P. F. McMillan, A. Gavriilidis, *Catal. Today* 126 (2007) 119.
- [49] X. D. Wang, W. T. Tysoe, R. G. Greenler, K. Truszkowska, *Surf. Sci.* 258 (1991) 335.
- [50] X. Bao, J. V. Barth, G. Lehmppfuhl, R. Schuster, Y. Uchida, R. Schlogl, G. Ertl, *Surf. Sci.* 284 (1993) 14.
- [51] G. Cipriani, D. Loffreda, A. Corso, S. de Gironcoli, S. Baroni, *Surf. Sci.* 501 (2002) 182.
- [52] M. R. Salazar, C. Saravanan, J. D. Kress, A. Redondo, *Surf. Sci.* 449 (2000) 75.
- [53] E. German, I. Efremenko, *Journal of Molecular Structure: THEOCHEM* 711 (2004) 159.
- [54] David Loffreda, Andrea Dal Corso, Stefano Baroni, Letizia Savio, Luca Vattuone, M. Rocca, *Surface Science* 530 (2003)
- [55] A. Kokalj, P. Gava, S. de Gironcoli, S. Baroni, *J. Phys. Chem. C* 112 (2008) 1019.
- [56] W.-L. Yim, T. Kluner, *J. Catal.* 254 (2008) 349.
- [57] D. Torres, N. Lopez, F. Illas, R. Lambert, *Angew. Chem. Int. Ed.* 46 (2007) 2055.
- [58] A. Roldan, D. Torres, J. M. Ricart, F. Illas, *J. Mol. Catal. A: Chem.* 306 (2009) 6.
- [59] L. M. Molina, S. Lee, K. Sell, G. Barcaro, A. Fortunelli, B. Lee, S. Seifert, R. E. Winans, J. W. Elam, M. J. Pellin, I. Barke, V. von Oeynhausen, Y. Lei, R. J. Meyer, J. A. Alonso, A. F. Rodriguez, A. Kleibert, S. Giorgio, C. R. Henry, K. H. Meiwes-Broer, S. Vajda, *Catal. Today* 160 (2011)
- [60] F. D. Murnaghan, *Proc. Natl. Acad. Sci. U. S. A.* 30 (1944) 244.
- [61] F. Birch, *Physical Review* 71 (1947) 809.
- [62] J. P. Perdew, Y. Wang, *Phys. Rev. B* 45 (1992) 13244.

- [63] J. P. Perdew, J. A. Chevary, S. H. Vosko, K. A. Jackson, M. R. Pederson, D. J. Singh, C. Fiolhais, *Phys. Rev. B* 46 (1992) 6671.
- [64] P. E. Blöchl, *Phys. Rev. B* 50 (1994) 17953.
- [65] G. Kresse, D. Joubert, *Phys. Rev. B* 59 (1999) 1758.
- [66] G. Henkelman, H. Jonsson, *The Journal of Chemical Physics* 111 (1999) 7010.
- [67] G. Kresse, J. Furthmüller, *Phys. Rev. B* 54 (1996) 11169.
- [68] A. Becke, *The Journal of Chemical Physics* 98 (1993) 5648.
- [69] C. Lee, W. Yang, R. Parr, *Phys. Rev. B* 37 (1988) 785.
- [70] J. Čížek, *Adv. Chem. Phys.* (2007) 35.
- [71] G. Purvis, R. Bartlett, *The Journal of Chemical Physics* 76 (1982) 1910.
- [72] D. Andrae, U. Häußermann, M. Dolg, H. Stoll, H. Preuß, *Theoretical Chemistry Accounts: Theory, Computation, and Modeling (Theoretica Chimica Acta)* 77 (1990) 123.
- [73] I. Antes, S. Dapprich, G. Frenking, P. Schwerdtfeger, *Inorg. Chem.* 35 (1996) 2089.
- [74] M. Frisch, J. Pople, S. Binkley, *The Journal of Chemical Physics* 80 (1984) 3265.
- [75] M. J. Frisch, G. W. Trucks, H. B. Schlegel, G. E. Scuseria, M. A. Robb, J. R. Cheeseman, G. Scalmani, V. Barone, B. Mennucci, G. A. Petersson, H. Nakatsuji, M. Caricato, X. Li, H. P. Hratchian, A. F. Izmaylov, J. Bloino, G. Zheng, J. L. Sonnenberg, M. Hada, M. Ehara, K. Toyota, R. Fukuda, J. Hasegawa, M. Ishida, T. Nakajima, Y. Honda, O. Kitao, H. Nakai, T. Vreven, J. J. A. Montgomery, J. E. Peralta, F. Ogliaro, M. Bearpark, J. J. Heyd, E. Brothers, K. N. Kudin, V. N. Staroverov, R. Kobayashi, J. Normand, K. Raghavachari, A. Rendell, J. C. Burant, S. S. Iyengar, J. Tomasi, M. Cossi, N. Rega, J. M. Millam, M. Klene, J. E. Knox, J. B. Cross, V. Bakken, C. Adamo, J. Jaramillo, R. Gomperts, R. E. Stratmann, O. Yazyev, A. J. Austin, R. Cammi, C. Pomelli, J. W. Ochterski, R. L. Martin, K. Morokuma, V. G. Zakrzewski, G. A. Voth, P. Salvador, J. J. Dannenberg, S. Dapprich, A. D. Daniels, Ö. Farkas, J. B. Foresman, J. V. Ortiz, J. Cioslowski, D. J. Fox; Gaussian Inc.: Wallingford CT, 2009.
- [76] S. Grimme, J. Antony, S. Ehrlich, H. Krieg, *The Journal of Chemical Physics* 132 (2010) 154104.
- [77] Grimme web.
- [78] N. Iwasaki, Y. Sasaki, Y. Nishina, *Surf. Sci.* 198 (1988) 524.
- [79] L. Molina, S. Lee, K. Sell, G. Barcaro, A. Fortunelli, B. Lee, S. Seifert, R. Winans, J. Elam, M. Pellin, I. Barke, V. Oeynhausien, Y. Lei, R. Meyer, J. Alonso, A. Fraile Rodríguez, A. Kleibert, S. Giorgio, C. Henry, K.-H. Meiwes-Broer, S. Vajda, *Catal. Today* 160 (2011)
- [80] J. Chou, E. W. McFarland, *Chem. Commun.* (2004) 1648.
- [81] K. A. Davis, D. W. Goodman, *J. Phys. Chem. B* 104 (2000) 8557.

**Table 1.** Product distribution obtained by mass spectrometry at different temperatures on Ag(100) and Ag(111) monocrystals.<sup>a</sup>

m/z <sup>b</sup>	Product <sup>c</sup>	Ag(100)			Ag(111)		
		200 <sup>d</sup>	250 <sup>d</sup>	275 <sup>d</sup>	200 <sup>d</sup>	250 <sup>d</sup>	275 <sup>d</sup>
M31	P. Oxide/Propanal	0.07	0.29	0.26	0	0	0
M43	Acetone	0.07	0.24	0.26	0	0	0
M44	CO <sub>2</sub>	1	1	1	1	1	1
M56	Acrolein	0.29	0.38	0.44	0	0	0

<sup>a</sup> Calculated as yield of product/yield of CO<sub>2</sub> at conversion < 1%.

<sup>b</sup> m/z used in the product identification.

<sup>c</sup> Molecule(s) assigned to m/z.

<sup>d</sup> Reaction temperature, in °C.

## Figure Captions

**Scheme 1.** Schematic reaction mechanism for propene epoxidation on Ag catalyst.

**Figure 1.** Periodic PW91 optimized structures for: i) bare silver (100) (a) and (111) (e) surfaces, ii) O<sub>2</sub> adsorption complex over Ag(100) (b) and Ag(111) (f) surface models, iii) transition state structure on Ag(100) (c) and Ag(111) (g) surface models, and iv) oxygen adatoms over Ag(100) (d) and Ag(111) (h) surfaces. Ag and O atoms are depicted as blue and red spheres, respectively. For silver atoms, deeper surface shells are shown with lighter blue colors.

**Figure 2.** Relative energies calculated at the B3LYP-D3 level of the species involved in the mechanism of O<sub>2</sub> dissociation over Ag(100) and Ag(111) surfaces, and optimized geometries of reaction intermediates and transition states structures. Ag and O atoms are depicted in blue and red, respectively. For the sake of clarity only the first layer of the Ag surfaces is shown.

**Figure 3.** Evolution of the bands in Raman spectra after O<sub>2</sub> adsorption on a) Ag(111) and b) Ag(100) surfaces at 200 °C (green line), 225 °C (black line) and 250 °C (red line) and after flow of an inert gas (blue line).

**Figure 4.** Periodic PW91 optimized geometries of the intermediates and transition state structures along the reaction pathways for propylene oxidation over Ag(100) surface.

**Figure 5.** Relative energies calculated at the B3LYP-D3 level along the reaction pathways for propylene oxidation over a) Ag(100) and b) Ag(111) surfaces. The *allyl* route is depicted in red, the *branched* routes leading to acetone (dashed line) and epoxide (full line) are depicted in green, and the *linear* routes leading to propanal (dashed line) and epoxide (full line) are depicted in blue.

**Figure 6.** Periodic PW91 optimized geometries of the intermediates and transition state structures along the reaction pathways for propylene oxidation over Ag(111) surface.

**Figure 7.** Evolution of the bands in the Raman spectra on: a) Ag(111) and b) Ag(100) surfaces in a 20% O<sub>2</sub>/Ar flow at 200 °C (green line), in a C<sub>3</sub>H<sub>6</sub>/O<sub>2</sub>/Ar flow at 200 °C (red line), and in a C<sub>3</sub>H<sub>6</sub>/O<sub>2</sub>/Ar flow at 250 °C (black line).